

OPEN

# The serum amyloid A3 promoter-driven luciferase reporter mice is a valuable tool to image early renal fibrosis development and shows the therapeutic effect of glucosyl-hesperidin treatment

Thanutchaporn Kumrungsee<sup>1</sup>, Taishi Kariya<sup>1</sup>, Kotaro Hashimoto<sup>1</sup>, Takayuki Koyano<sup>2</sup>, Nao Yazawa<sup>1</sup>, Takao Hashimoto<sup>1</sup>, Yohei Sanada<sup>1</sup>, Makoto Matsuyama<sup>2</sup>, Yusuke Sotomaru<sup>3</sup>, Hiroaki Sakurai<sup>4</sup>, Fons A. J. van de Loo<sup>5</sup> & Noriyuki Yanaka<sup>1</sup>

Tubulointerstitial fibrosis is a progressive process affecting the kidneys, causing renal failure that can be life-threatening. Thus, renal fibrosis has become a serious concern in the ageing population; however, fibrotic development cannot be diagnosed early and assessed noninvasively in both patients and experimental animal models. Here, we found that serum amyloid A3 (Saa3) expression is a potent indicator of early renal fibrosis; we also established *in vivo* Saa3/C/EBP $\beta$ -promoter bioluminescence imaging as a sensitive and specific tool for early detection and visualization of tubulointerstitial fibrosis. Saa3 promoter activity is specifically upregulated in parallel with tumor necrosis factor  $\alpha$  (TNF- $\alpha$ ) and fibrotic marker collagen I in injured kidneys. C/EBP $\beta$ , upregulated in injured kidneys and expressed in tubular epithelial cells, is essential for the increased Saa3 promoter activity in response to TNF- $\alpha$ , suggesting that C/EBP $\beta$  plays a crucial role in renal fibrosis development. Our model successfully enabled visualization of the suppressive effects of a citrus flavonoid derivative, glucosyl-hesperidin, on inflammation and fibrosis in kidney disease, indicating that this model could be widely used in exploring therapeutic agents for fibrotic diseases.

About 750 million people suffer from chronic kidney disease (CKD) with global deaths predicted to rise from 1.2 million in 2016 to 3.1 million in 2040<sup>1,2</sup>. CKD causes progressive decline in both kidney function and structure without obvious outward symptoms, making it difficult to diagnose until end stage where it is irreversible and requires dialysis or kidney transplantation to maintain patients' lives, which is an economic burden for developing countries<sup>2-4</sup>. Thus, effective disease assessment at early stages is essential in order to improve diagnosis and prognosis and to provide prompt treatment before the onset of end-stage renal disease. Renal fibrosis, particularly tubulointerstitial fibrosis, is a hallmark of end-stage kidney disease<sup>5,6</sup>. Molecular mechanisms of tubulointerstitial fibrosis involve tubular epithelial cells, a primary target of renal injurious stimuli, being injured by intratubular hydrodynamic forces, such as tubular stretch induced by obstruction; which activates inflammatory and fibrogenic signals<sup>5-7</sup>. Together with the alteration of tubular epithelial phenotype, these signals lead to activation of tubulointerstitial fibroblasts and myofibroblasts, resulting in deposition of extracellular matrix (ECM), such as

<sup>1</sup>Graduate School of Biosphere Science, Hiroshima University, Higashi-Hiroshima, Japan. <sup>2</sup>Division of Molecular Genetics, Shigei Medical Research Institute, 2117 Yamada, Minami-ku, Okayama, Japan. <sup>3</sup>Natural Science Center for Basic Research and Development, Hiroshima University, Hiroshima, Japan. <sup>4</sup>Department of Cancer Cell Biology, Graduate School of Medicine and Pharmaceutical Sciences, University of Toyama, Toyama, Japan. <sup>5</sup>Experimental Rheumatology, Department of Rheumatology, Radboud University Medical Center, Nijmegen, The Netherlands. Correspondence and requests for materials should be addressed to Thanutchaporn Kumrungsee (email: [kumrung@hiroshima-u.ac.jp](mailto:kumrung@hiroshima-u.ac.jp)) or Noriyuki Yanaka (email: [yanaka@hiroshima-u.ac.jp](mailto:yanaka@hiroshima-u.ac.jp))

collagen in interstitial areas, finally leading to tubulointerstitial fibrosis. At the transcriptional level, in response to injuries, transcriptional factors that regulate expression of genes involved in fibrosis, such as  $\alpha$ -smooth muscle actin ( $\alpha$ SMA), are activated. In addition to myofibroblasts, recent studies have suggested that renal tubular epithelial cells are an important initiator and mediator of tubulointerstitial fibrosis and attempted to isolate marker proteins in injured tubular epithelial cells to serve as indicators for early detection of tubulointerstitial fibrosis<sup>8,9</sup>.

In a few decades, *in vivo* imaging technologies have become essential for the basic sciences and for translational drug development because they provide an important opportunity for studying biological processes in living organisms in real time at a molecular level. Recently, imaging devices have been developed to gain high-resolution bioluminescence images of luciferase or fluorescence proteins and are applicable for studying not only tumorigenesis but also inflammatory diseases and other pathologies<sup>10,11</sup>. In our previous study, we successfully used a mouse serum amyloid A3 (Saa3) gene promoter-luciferase (luc) reporter to monitor inflammation in fat tissue of obese mice<sup>12</sup>. Saa3 is a member of the Saa family, which comprises of acute-phase proteins highly expressed under various inflammatory conditions and whose mRNA expression profiles in chronic inflammatory diseases, such as rheumatoid arthritis, atherosclerosis, and colitis, have been studied<sup>13–15</sup>. In the mouse Saa3 gene promoter region, there are three CCAAT/enhancer binding protein  $\beta$  (C/EBP $\beta$ )-binding sites (–152, –107, and –77)<sup>12,13,16</sup>. C/EBP $\beta$  is transcriptionally activated by inflammatory stimuli, including inflammatory cytokines, such as interleukin-6 (IL-6), IL-1, and tumor necrosis factor  $\alpha$  (TNF- $\alpha$ ), and the possibility that C/EBP $\beta$  may play an important role in inflammatory signals during disease development has been explored<sup>12,13,17–19</sup>. In addition, there is an upregulation of the Saa family proteins in serum and kidney tissue of both patients and experimental animals having kidney disease<sup>20–25</sup>. Taken together, these observations indicate that C/EBP $\beta$  and its regulated Saa family of genes may represent an important target for assessing kidney injury and the Saa3-promoter reporter might be used in live animals for visualizing the injury in experimental kidney disease models and for monitoring therapeutic effects of functional food on the pathology of diseases.

Here, we report that *in vivo* Saa3/C/EBP $\beta$ -promoter bioluminescence imaging is a novel, sensitive, and specific approach for detecting and visualizing tubulointerstitial injury and fibrosis as well as monitoring the therapeutic effect of functional food on kidney disease. In fact, our *in vivo* bioluminescence imaging model revealed a functional food, which shows preventive effect on kidney disease. Importantly, we also report here that C/EBP $\beta$  plays a crucial role in renal tubulointerstitial injury and fibrosis, possibly by driving the fibrotic marker Saa3. As C/EBP $\beta$  is likely to be an upstream regulator for tubulointerstitial fibrosis, our finding may open the door to the design of future therapeutic strategies or screening for novel therapeutic functional food by controlling the levels of expression of C/EBP $\beta$ .

## Results

**Upregulation of Saa3 promoter activity in adenine-induced kidney injury.** To determine if the Saa3-promotor (–314/+50) reporter is useful for assessing kidney injury, we employed transgenic mice carrying the Saa3 promoter-luc chimeric gene. Since the transgenic mice showed high Saa3 promoter activity in kidney tissue under normal conditions (Supplementary Fig. S1a), it is logical to examine the luciferase activity based on Saa3 promoter activity during kidney disease development by *in vivo* imaging technique. In order to induce injury in kidney, mice were fed the adenine-containing diet for three weeks. We found that blood urea nitrogen (BUN) and plasma creatinine concentrations in the adenine group were significantly increased as compared to the control group (Fig. 1a,b). Pathological changes in the adenine-induced kidney were observed using hematoxylin-eosin (H&E) and Azan-Mallory (AZM) staining; deposition of 2,8-dihydroxyadenine (DHA) crystals in renal tubules (brown), expansion of interstitial ECM, and accumulation of collagen, which are typical pathologies of tubulointerstitial fibrosis, were observed after three weeks, while abnormal tubular dilation and atrophy appeared after one week of the adenine diet (Supplementary Fig. S2). We further observed that Saa3 mRNA expression was greatly upregulated (13-fold,  $p < 0.05$ ) in the kidney tissue of adenine-fed mice (Fig. 1c). Next, to employ the *in vivo* Saa3 promoter-luc model for monitoring the kidney injury, Saa3 promoter-luc mice were divided into two groups receiving the adenine diet or the control diet and subjected to *in vivo* bioluminescent analysis. Shortly after one week of feeding, *in vivo* bioluminescence imaging from the back of Saa3 promoter-luc mice showed that injured kidneys emitted a strong bioluminescent signal (from violet for least intense to red for most intense), while uninjured kidneys of the mice fed the control diet showed none or less bioluminescent signal (Fig. 1d). To confirm that the visualized Saa3 promoter activity or the bioluminescent signal was specifically generated from the injured kidneys, we opened up the belly of Saa3 promoter-luc mice that were fed the adenine diet or the control diet and subjected them to the *in vivo* bioluminescent analysis. As shown in Fig. 1e, a very intense bioluminescent signal was specifically observed from the adenine-induced injured kidney (the white arrow), and not from the adjacent organs, whereas the uninjured kidneys and the other organs of the mice that were fed the control diet showed no bioluminescent signal. This *in vivo* result is consistent with the *ex vivo* result demonstrating that the adenine-induced injured kidney tissue exhibited a higher Saa3 promoter activity (luciferase activity) than the non-adenine-induced kidney tissue (3.5-fold,  $p < 0.01$ , Fig. 1f). In addition, upon adenine induction, kidney tissue showed a higher Saa3 promoter activity than other organ tissues (Supplementary Fig. S1b). These results indicated that the bioluminescent signal observed in Saa3 promoter-luc mice specifically reflected kidney injury. To assess the correlation of Saa3 promoter activity with mRNA expressions of Saa3, a fibrotic marker (collagen I (Coll)), and an inflammatory marker (TNF- $\alpha$ ) in the injured kidneys from the tissue lysate was subjected to qualitative RT-PCR analysis and Pearson's correlation coefficient analysis. Saa3 mRNA expression levels in the injured kidneys actually exhibited a positive correlation with Saa3 promoter activity ( $r = 0.729$ ,  $p < 0.05$ , Fig. 1g). Importantly, mRNA expression levels of Coll and TNF- $\alpha$  were positively correlated with Saa3 promoter activity ( $r = 0.997$ ,  $p < 0.05$ ;  $r = 0.991$ ,  $p < 0.05$ , respectively; Supplementary Fig. S3a,b). In addition to these, a significant correlation between Saa3 promoter activity with transforming growth factor beta 1 (TGF- $\beta$ 1) ( $r = 0.980$ ,  $p < 0.05$ , Supplementary Fig. S3c) was found. These results suggested that an increase in

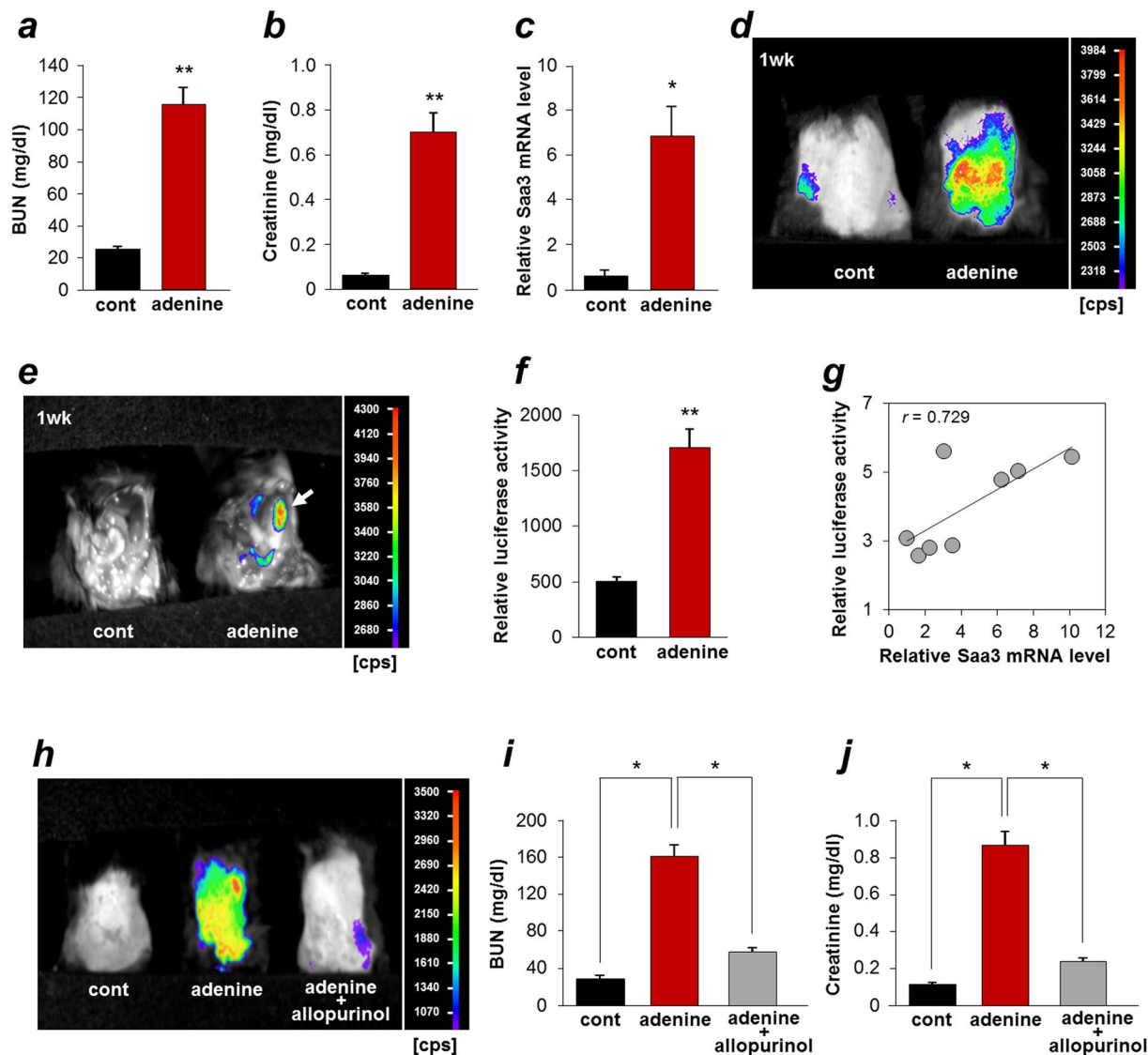


**Figure 1.** Bioluminescence imaging allows visualization of adenine-induced tubulointerstitial injury and fibrosis in Saa3 promoter-luc mice. (a–c) Wide-type mice were divided into two groups ( $n = 4$ ) receiving the control diet (cont) or the adenine diet (adenine) for 3 weeks. (a) Plasma BUN and (b) creatinine levels were increased by the adenine diet ( $n = 4$ ). (c) The relative Saa3 mRNA level in kidney tissues was determined by quantitative PCR and normalized to L19 mRNA level ( $n = 4$ ). (d–k) Saa3 promoter-luc mice were divided into two groups ( $n = 4$ ) receiving the control diet (cont) or the adenine diet (adenine) for one week. (d) *In vivo* bioluminescence imaging from the back of Saa3 promoter-luc mice that were fed the adenine diet shows a strong intensity of bioluminescent signal (from violet for least intense to red for most intense), reflecting kidney injury. (e) Exposure of mouse organs under *in vivo* bioluminescent analysis exhibited a very intense bioluminescent signal generated specifically from the injured kidney (the white arrow), and not from the adjacent organs of the mice that were fed the adenine diet. (f) Kidney tissues were isolated and subjected to the *ex vivo* luciferase activity assay to show enhancement of bioluminescent signal intensity induced by the adenine diet ( $n = 4$ ). (g) The relative Saa3 mRNA expression level in kidney tissue was determined by quantitative PCR and normalized to L19 mRNA level ( $n = 4$ ). Pearson's correlation coefficient showed a positive correlation between luciferase activity (promoter activity) and Saa3 mRNA expression level in kidney tissue. (h–j) The treatment with allopurinol of Saa3 promoter-luc mice ( $n = 3$ ) receiving the adenine diet for six weeks. (h) The *in vivo* bioluminescence imaging shows decreased signal intensity in the adenine-induced mouse treated with allopurinol, reflecting less severe injury in kidney, as compared with the adenine-induced mouse without allopurinol treatment. (i,j) Allopurinol decreased plasma BUN and creatinine levels in the adenine-induced mice ( $n = 3$ ). All values are expressed as mean  $\pm$  S.E. Student's *t*-test, \* $p < 0.05$ , \*\* $p < 0.01$ .

Saa3 promoter activity was possibly associated with tubulointerstitial fibrosis and inflammation occurring in adenine-induced kidney disease. In this study, one week of the adenine diet did not change BUN and plasma creatinine concentration (Supplementary Fig. S4), and deposition of DHA crystals was not observed in renal tubules

(Supplementary Fig. S2a). However, replacement of connective tissue began after only one week of the adenine diet (Supplementary Fig. S2b). Taken together, these results indicated a potential ability of the *in vivo* bioluminescence imaging from Saa3 promoter-luc mice to predict tubulointerstitial fibrosis at an early phase.

To verify the reliability of this Saa3 promoter-luc mouse model as a tool for monitoring kidney injury and tubulointerstitial fibrosis, we applied this model to assess the therapeutic effect of allopurinol, a xanthine dehydrogenase inhibitor as a positive control drug<sup>26</sup>, on adenine-induced kidney injury. As shown in Fig. 1h, there was no bioluminescent signal in the control group, reflecting uninjured kidney, but a strong signal intensity in the adenine group, indicating severely injured kidneys, and a decrease in the signal intensity in the adenine group treated with allopurinol, reflecting less severe injury of the kidney, due to the therapeutic effect of allopurinol. These *in vivo* bioluminescent results were confirmed by biochemistry results, in which plasma BUN and creatinine concentrations in the adenine group were significantly increased as compared to the control group but were significantly decreased by allopurinol treatment (Fig. 1i,j). Taken together, the Saa3 promoter-luc mouse model established in this study is a non-invasive and useful tool for visualizing progressive kidney injury and possibly predicting tubulointerstitial fibrosis in the early stage in live animals.

**Upregulation of Saa3 promoter activity in a unilateral ureteral obstruction model.** To confirm if the Saa3 promoter-luc mouse model can be used to detect acute tubulointerstitial injury and predict tubulointerstitial fibrosis, we applied unilateral ureteral obstruction (UUO), that is an acute and well-established model of tubulointerstitial injury/fibrosis, in this study<sup>5</sup>. Saa3 promoter-luc mice were operated, and their left kidneys were ligated to obstruct the flow of urine, while their right kidneys were left unligated. Shortly after 3 days of the UUO operation, we subjected the mice to *in vivo* bioluminescent analysis and found that the ligated kidneys (left side indicated as “L” in Fig. 2a) showed stronger intensity of the bioluminescent signal than the unligated kidneys (right side indicated as “R” in Fig. 2a), while Saa3 promoter-luc mice with sham operation exhibited no bioluminescent signal in both the kidneys (Supplementary Fig. S5). These results suggested that acute tubulointerstitial injury, specifically upregulated Saa3 promoter activity, and higher Saa3 promoter activity visualized in ligated kidneys indicated greater severity of tubulointerstitial injury than that in unligated kidneys and sham-operated kidneys. To confirm this, kidney tissues were isolated, lysed, and subjected to the *ex vivo* quantitative luciferase assay. As compared with the basal Saa3 promoter activity from uninjured kidneys (cont), Saa3 promoter activity was increased in parallel with greater severity of tubulointerstitial injury in unligated kidneys (R) and ligated kidneys (L), respectively (Fig. 2b). Notably, the bioluminescent signal and Saa3 promoter activity observed in unligated kidneys (R) shown in Fig. 2a,b is possibly from hyperfiltration of unligated kidneys, due to the ligation of the left kidney. Subsequently, the hyperfiltration of unligated kidneys might result in intratubular hydrodynamic forces triggering inflammatory and fibrogenic signals<sup>5</sup>, which, in turn, caused upregulation of Saa3 promoter activity. In fact, the unligated right kidneys showed higher mRNA expression level of ColI,  $\alpha$ SMA, and TGF $\beta$  compared with kidneys from control mice (Supplementary Fig. S6). Next, we further assessed mRNA expressions of Saa3, fibrotic markers, and inflammatory markers by subjecting the tissues of sham-operated and ligated or UUO kidneys after three days of the operation to qRT-PCR analyses and found that increased mRNA expressions of Saa3, ColI,  $\alpha$ SMA, TGF- $\beta$ , TNF- $\alpha$ , and EGF-like module containing mucin-like hormone receptor1 (Emr1) were clearly seen in UUO kidneys than in sham-operated kidneys (Fig. 2c). Immunohistochemical analyses revealed that severe tubulointerstitial damage was present after seven days of the UUO operation (Fig. 2e), as reflected by a highly increased  $\alpha$ SMA expression and reduction of E-Cad expression compared with those from three day UUO kidneys (Fig. 2d). However, Saa3 promoter activity as well as mRNA expression of Saa3, ColI,  $\alpha$ SMA, and TNF- $\alpha$  was upregulated early in tubulointerstitial injury (three days). In the UUO kidneys after three days of the operation, dilated tubules were observed and  $\alpha$ SMA-positive area was moderately increased (Supplementary Fig. S7). These observations suggest that the Saa3 promoter-luc mouse model can be used to detect tubulointerstitial injury and predict fibrosis in the early stage.

**C/EBP $\beta$  plays a crucial role in controlling Saa3 promoter activity.** In this study, we aimed to determine a possible role of the transcription factor, C/EBP $\beta$  in kidney injury and fibrosis by monitoring Saa3 promoter activity. First, we examined if C/EBP $\beta$  is upregulated in injured kidneys by subjecting the tissue lysates of the adenine- and UUO-treated kidneys to qRT-PCR and western blot analyses. As shown in Fig. 3a,b, C/EBP $\beta$  mRNA and protein expressions were highly increased in both adenine-treated and ligated kidneys (L) compared with uninjured kidneys in the control group (cont) and unligated kidneys (R). Taken together with the results demonstrating an upregulation of Saa3 mRNA expression and Saa3 promoter activity in the adenine- and UUO-treated kidneys (Figs 1 and 2), these results suggested a possible relationship between C/EBP $\beta$  and Saa3 expression in kidney injury. To determine which cells are responsible for C/EBP $\beta$  expression in injured kidneys, serial sections of the adenine-treated kidneys were analyzed by immunohistochemical analysis. As shown in Fig. 3c, C/EBP $\beta$  localized specifically in tubular epithelial cells, confirmed by having the same localization with E-Cad, a specific surrogate marker of renal tubular epithelial cells<sup>27</sup>. Given this, we carried out experiments using human renal tubular epithelial cell line HK-2 to confirm direct regulation of the Saa3 promoter activity by C/EBP $\beta$ . Upon transfection into HK-2 cells carrying Saa3 promoter-luc gene, overexpression of C/EBP $\beta$  remarkably increased Saa3 promoter activity, which was further enhanced by the addition of TNF- $\alpha$ , an inflammatory stimulus reported to activate C/EBP $\beta$ <sup>12</sup> (Fig. 3d). C/EBP $\beta$ -binding sites are located at -152, -107, and -77 bp upstream of the transcription start site in the Saa3 promoter (Fig. 3e)<sup>12,13,16</sup>. Thus, we constructed three Saa3 promoter mutants at those three binding sites and the wild-type (WT) Saa3 promoter (Fig. 3e) to determine whether these C/EBP $\beta$ -binding sites are important for Saa3 promoter regulation. After transfection into HK-2 cells, both the WT and mutant construct I (-77) exhibited a 2-fold increase in luciferase activity in response to TNF- $\alpha$ , while mutant constructs II (-107) and III (-152) abolished luciferase activity upon TNF- $\alpha$  treatment (Fig. 3f). These results strongly indicated that C/EBP $\beta$  played a crucial role in regulation of Saa3 promoter activity, specifically



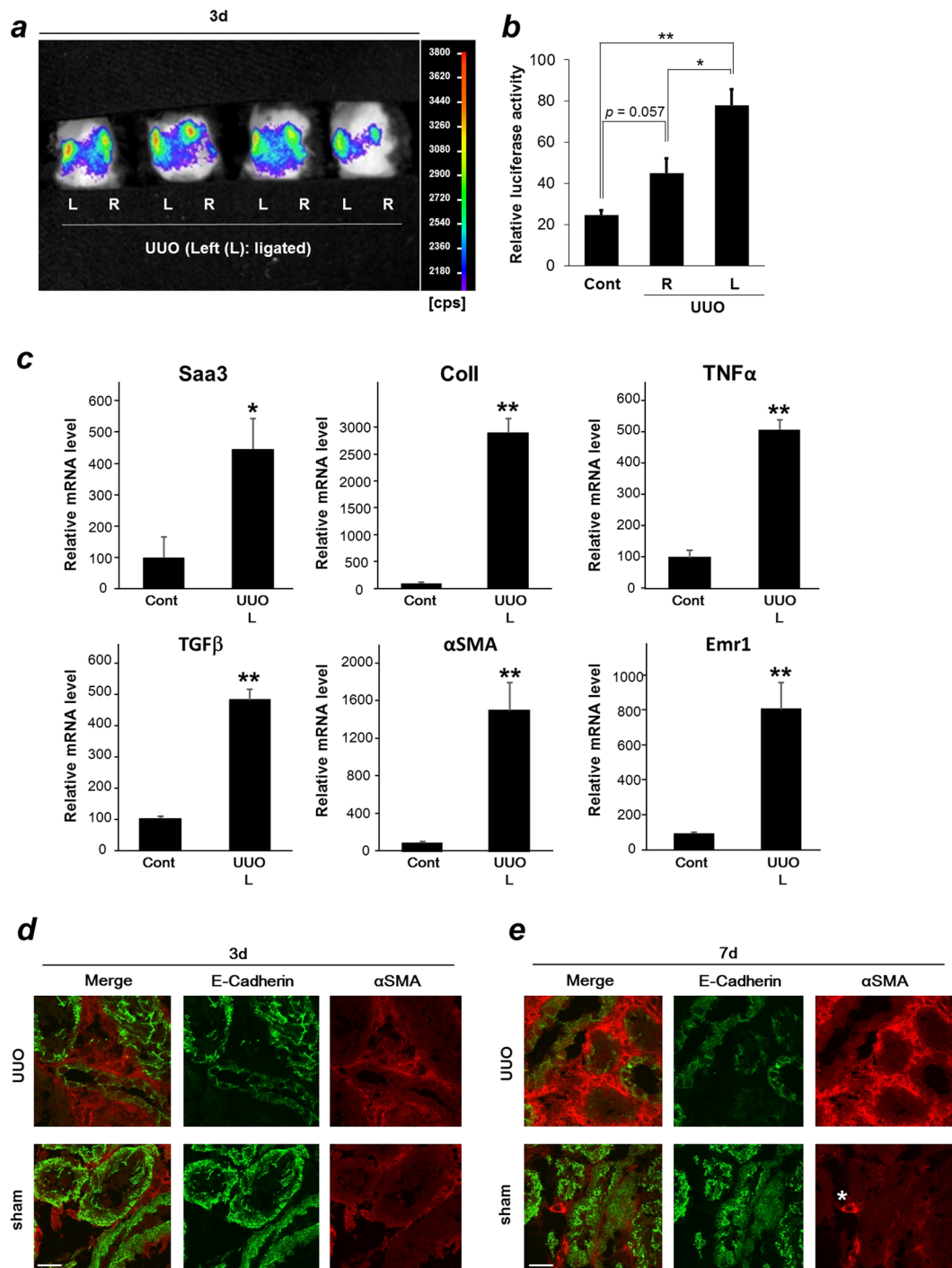


**Figure 2.** Bioluminescence imaging allows early prediction of tubulointerstitial injury and fibrosis in Saa3 promoter-luc mice under unilateral ureteral obstruction. (a–c) Saa3 promoter-luc mice were under unilateral ureteral obstruction (UUO) for 3 days ( $n = 4$ ). Left ureters of the mice were ligated for three days (“L” represents left side and ligated kidneys), while right ureters were left without the ligation (“R” represents right side). (a) The *in vivo* bioluminescence imaging showed a stronger intensity of bioluminescent signal in the ligated kidneys (L) than in the unligated kidneys (R). (b) Kidney tissues were isolated and subjected to the *ex vivo* luciferase activity assay to show upregulation of Saa3 promoter activity in the ligated kidneys (L), as compared with the unligated kidneys (R) and control kidneys without the operation (cont) ( $n = 4$ ). (c) mRNA levels of Saa3, Coll, TNF- $\alpha$ , TGF $\beta$ ,  $\alpha$ SMA and Emr1 in left kidney tissues of the sham (Cont) and UUO mice (UUO L) were analyzed by quantitative RT-PCR and normalized to L19 mRNA level ( $n = 5$ ). (d,e) Wild-type mice were divided into two groups with sham operation or UUO operation. Mice were sacrificed at three or seven days after the operation. (d) and (e) Immunohistochemical staining shows expressions of E-Cad and  $\alpha$ SMA in sham and UUO kidneys after three and seven days of the operation, respectively.  $\alpha$ SMA protein is also expressed in the blood vessel and shown as a positive control by a star. Scale bar, 25  $\mu$ m. All values are expressed as mean  $\pm$  S.E. Student’s *t*-test,  $*p < 0.05$ ,  $**p < 0.01$ .

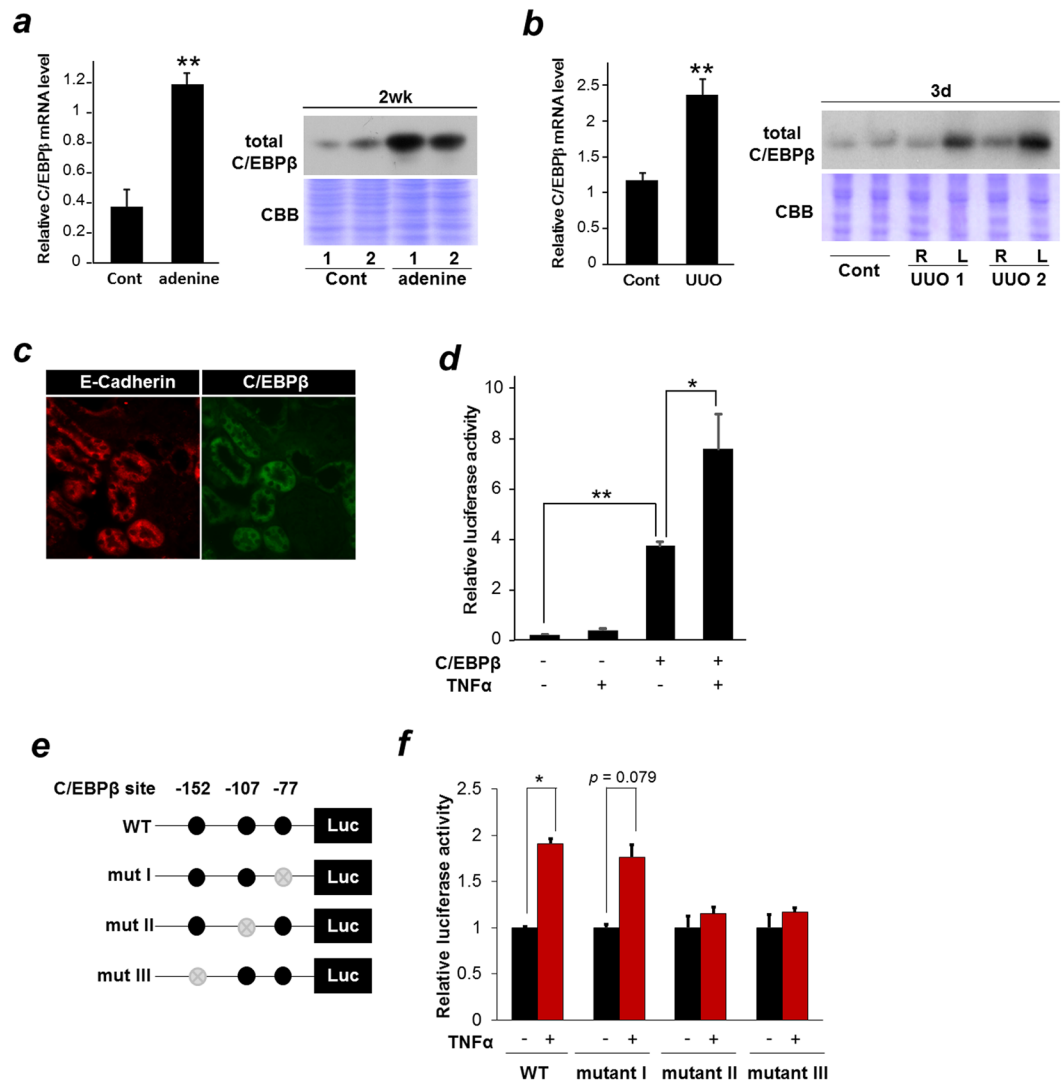


**Figure 3.** C/EBP $\beta$  is involved in regulating Saa3 promoter activity responsible for tubulointerstitial injury and fibrosis. **(a)** Wild-type (WT) mice were divided into two groups ( $n = 6$ ) receiving the control diet (cont) or the adenine diet (adenine) for two weeks. The relative C/EBP $\beta$  mRNA expression level in kidney tissue was determined by quantitative PCR and normalized to L19 mRNA level ( $n = 4$ ). Then, kidney tissues were isolated, lysed, and subjected to western blot analysis to determine C/EBP $\beta$  protein level ( $n = 2$ ). **(b)** Left ureters of WT mice in the unilateral ureteral obstruction (UUO) group were ligated for three days (“L” represents left side), while right ureters were left without the ligation (“R” represents right side). The control group without the operation was used to compare with the UUO group. The relative C/EBP $\beta$  mRNA expression level in kidney tissue was determined by quantitative PCR and normalized to L19 mRNA level ( $n = 5$ ). Then, kidney tissues were isolated, lysed, and subjected to western blot analysis to determine CEBP $\beta$  protein level ( $n = 2$ ). **(c)** Immunohistochemical staining shows expressions of E-Cad and CEBP $\beta$  in kidney tissues from WT mice under the adenine diet for two weeks. **(d)** HK-2 cells were transiently transfected with constructs for Saa3-luc with pcDNA-C/EBP $\beta$  or empty vector. Two days after transfection, cells were treated with 10 ng/ml of TNF- $\alpha$  for 8 h, scraped and subjected to the luciferase assay. Data are means of triplicate experiments ( $n = 4$ ). **(e)** Saa3 promoter was mutated and ligated upstream of the complete luciferase cDNA, generating mutant Saa3 promoter-luciferase chimeric genes (mut I, mut II, and mut III), respectively. **(f)** HK-2 cells were treated with 10 ng/ml of TNF- $\alpha$  for 8 h, followed by the luciferase assay. The data are from a single experiment carried out ( $n = 3$ ) and are representative of two independent experiments. Full-length gels and blots are included in Supplementary Fig. S11.

through the C/EBP $\beta$ -binding sites at  $-107$  and  $-152$  bp of the Saa3 promoter. To confirm this *in vivo*, we analyzed the correlation between Saa3 promoter activity and C/EBP $\beta$  mRNA level in the adenine-treated kidney tissue by using Pearson’s correlation coefficient analysis and found that there was a significant correlation between Saa3 promoter activity and C/EBP $\beta$  mRNA level ( $r = 0.997$ ,  $p < 0.05$ , Supplementary Fig. S8). In addition, C/EBP $\beta$  mRNA level was found to be significantly correlated with ColII mRNA level ( $r = 0.979$ ,  $p < 0.05$ , Supplementary Fig. S8), suggesting a possible role of C/EBP $\beta$  in renal fibrosis. Taken with the previous results, the findings

implied that Saa3 promoter-luc mouse model could be used to reflect C/EBP $\beta$  activity in driving tubulointerstitial injury and fibrosis. To explore the biological significance of Saa3 expression in tubular epithelial cells, we used the siRNA-mediated the human homolog serum amyloid A (SAA1) knockdown in HK-2 cells. The amount of reduced mRNA expression was assessed by quantitative RT-PCR (Supplementary Fig. S9). Silencing of the SAA1 RNAi gene resulted in a decreased interleukin-8 (IL-8) mRNA expression in HK-2 cells (Supplementary Fig. S9). Because renal tubular epithelial cells are studied to produce inflammatory mediators, such as cytokines and chemokines, and actively participate in acute inflammatory processes by effecting and directing leukocyte chemotaxis via the production of IL-8<sup>28</sup>, these data suggest that SAA1 is actually involved in the early pathological process of kidney fibrosis and SAA1 serum levels might be useful assessing early stage human renal disease.

### Application of Saa3 promoter-luc mouse model in searching for functional food preventing kidney disease.

Citrus flavonoids have been reported to have protective kidney functions, including prevention of renal crystal formation<sup>29</sup>. In this study, we decided to use Saa3 promoter-luc mouse model for monitoring the potential preventive effect of citrus flavonoids on adenine-induced kidney disease. Since preliminary studies with certain types of flavonoids revealed a possibility of glucosyl-hesperidin (G-Hes) in preventing kidney injury, we subjected G-Hes to the *in vivo* bioluminescence imaging model. Transgenic mice were divided into three groups: the control group receiving the control diet, the adenine group receiving the adenine diet, and the G-Hes receiving the G-Hes-mixed adenine diet for one week. Three days prior to the treatment, the G-Hes group received the G-Hes diet, while the control and adenine groups received the control diet. After one week of the treatment, we subjected all mice to *in vivo* bioluminescent analysis. As shown in Fig. 4a, *in vivo* bioluminescence imaging showed strong signal intensity in the adenine group, indicating severely injured kidneys, and a decrease in the signal intensity in the G-Hes group (Supplementary Fig. S10a), indicating less severe injury of the kidneys, possibly due to the therapeutic effect of G-Hes, while no bioluminescent signal was observed in uninjured kidney of the control group (cont) that confirmed the specificity of Saa3 promoter activity to the injury. This result strongly suggested a preventive effect of G-Hes on adenine-induced kidney disease. To further confirm the preventive effect of G-Hes, after 3 weeks of the above treatment, all mice were sacrificed and subjected to further analyses. Figure 4b shows abnormal, ivory-white appearance of the adenine-treated kidney possibly due to DHA crystal accumulation, while the G-Hes treatment group showed usual appearance of kidney, suggesting the possibility of G-Hes in preventing DHA crystal formation. To observe morphological changes, the kidneys were sectioned and stained with Azan-Mallory stain. It appeared that G-Hes suppressed deposition of DHA crystals in renal tubules (brown), expansion of ECM, tubular dilation and atrophy, and tubulointerstitial fibrosis (blue), which were greatly present in the adenine group (Fig. 4c and Supplementary Fig. S10b,c). Consistent with histochemical staining results, G-Hes showed renal-protective effects by the significant reduction of plasma BUN and creatinine concentrations (Fig. 4d,e). Since G-Hes showed a potential suppression of DHA crystal formation in kidneys, we were interested in investigating the inhibitory effect of dietary G-Hes on activity of xanthine oxidoreductase (XOR), an enzyme responsible for conversion of adenine to DHA<sup>26</sup>. As shown in Fig. 4f, G-Hes suppressed XOR activity *in vivo*, indicated by the significant reduction of plasma levels of uric acid, a metabolic product of XOR, suggesting a possible renal protective effect of G-Hes through suppression of DHA crystal formation. To ensure that a reduction in plasma uric acid levels was due to the decreased activity of XOR by G-Hes and not by uricase, the uricase inhibitor, potassium oxonate, was applied during XOR activity assessment. Given that G-Hes is hydrolyzed to hesperetin by gut flora prior to being absorbed, we further confirmed the inhibitory effect of hesperetin on *in vitro* XOR activity from milk (IC<sub>50</sub> value was 10.6  $\mu$ M). Qualitative RT-PCR analysis revealed that G-Hes treatment downregulated mRNA expressions of Saa3, C/EBP $\beta$ , ColI,  $\alpha$ SMA, and TNF- $\alpha$  (Fig. 4g-k), indicating a possible role of G-Hes in suppressing inflammation and fibrosis in adenine-induced kidney disease. Taken together, the results suggested that G-Hes exerts its renal preventive effect through suppression of accumulation of DHA crystals in tubules via inhibition of XOR activity, thereby preventing tubular injury subsequent to reduction of inflammation, leading to prevention of further tubular injury and fibrosis in the kidneys. Notably, by exploiting the specificity of Saa3-promoter activity, this preventive effect could be visualized by bioluminescence imaging of live mice.

## Discussion

Scientific testing on animals has become a moral and social point of contention. In recent years, efforts have been made to reduce the number of experimental animals and to establish new non-invasive methods. *In vivo* bioluminescence imaging as a potent non-invasive assessment has been applied in various disease models, such as inflammation diseases and cancer metastasis<sup>11,12,30–32</sup>. However, until this point, this technology has not been utilized in kidney disease research. Examination by non-invasive imaging for renal fibrosis in both human and experimental animals, in particular, is nonexistent. Generally, tubulointerstitial fibrosis, a predictor of the progression of end-stage renal disease<sup>33</sup>, in patients is commonly assessed by biopsy and histological analysis<sup>5,6,33</sup>. Similarly, in experimental animals, analysis of tubulointerstitial fibrosis is often done by histochemical and/or gene and protein expression analyses, which require tissue or organ harvesting after sacrificing the animal; therefore, disease progression or therapeutic response in the same animal over time cannot be observed. To overcome these limitations, here we established and demonstrated that *in vivo* Saa3/C/EBP $\beta$ -promoter bioluminescence imaging is a sensitive and specific tool for detecting and visualizing tubulointerstitial injury in real time in live animals from both primary kidney disease models, adenine-derived, and UUO models. Moreover, this novel bioluminescence imaging has an advantage of early prediction of tubulointerstitial fibrosis, which cannot be detected or clearly distinguished by the typical and traditional histological analysis or blood markers such as BUN and creatinine at an early phase.

C/EBP $\beta$  is a transcription factor of various genes including Saa,  $\alpha$ SMA, and Col I<sup>12,13,17,18,34–36</sup>. C/EBP $\beta$  regulates expression of its target genes by binding to its binding sites in the promoter region of these genes subsequent

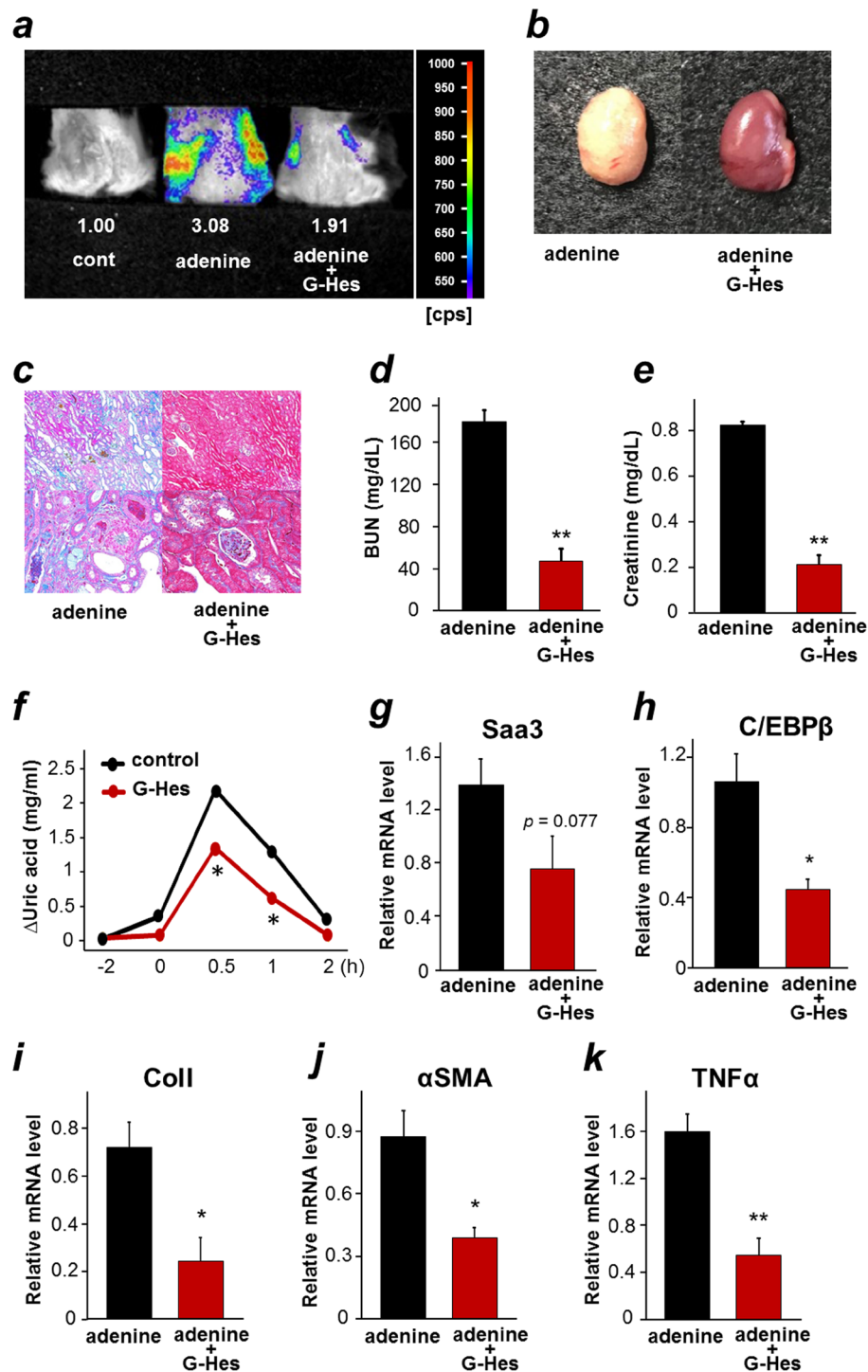


**Figure 4.** Bioluminescence imaging of Saa3 promoter-luc mice allows monitoring the response to glucosyl-hesperidin in adenine-induced kidney disease model. (a) The treatment of glucosyl-hesperidin (G-Hes) given to Saa3 promoter-luc mice receiving the adenine diet for one week. The *in vivo* bioluminescence imaging shows decreased signal intensity in the adenine-induced mouse treated with G-Hes, reflecting less severe injury in kidney, as compared with the adenine-induced mouse without G-Hes treatment. (b–e) Wild-type mice were divided into two groups ( $n = 6$ ) receiving the adenine diet (adenine) or the G-Hes-mixed adenine diet (adenine + G-Hes) for three weeks. (b) Appearance of kidneys in both groups. (c) Kidneys were sectioned and stained with Azan-Mallory to show morphological changes. (d) Plasma BUN and (e) creatinine levels were suppressed by the G-Hes treatment ( $n = 6$ ). (f) G-Hes treatment reduced plasma uric acid levels, exhibiting the inhibition of endogenous xanthine oxidoreductase (XOR) activity, ( $n = 5$ ). (g–k) The relative mRNA level of Saa3, C/EBP $\beta$ , Coll,  $\alpha$ SMA, and TNF- $\alpha$ , respectively, in kidney tissues of mice from the experiment in (b–e) was determined by quantitative PCR and normalized to L19 mRNA level ( $n = 6$ ). All values are expressed as mean  $\pm$  S.E. Student's *t*-test, \* $p < 0.05$ , \*\* $p < 0.01$ .



to gene transcription. Recently, C/EBP $\beta$  has been reported to play a crucial role in chronic inflammatory diseases, such as rheumatoid arthritis<sup>13,16</sup> and obesity<sup>12</sup>. Based on these findings, researchers have designed lentiviruses carrying Saa3/C/EBP $\beta$ -promoter reporter gene and used them as a sensitive tool for assessing arthritis and chronic inflammatory state in experimental animals<sup>12,13</sup>. In addition to involvement in chronic inflammatory diseases, recent emerging evidence has suggested a crucial role of C/EBP $\beta$  in fibrosis<sup>17,18,35,36</sup>. In lung and liver fibrosis, its mechanism of action works by controlling transcription of  $\alpha$ SMA and ColI genes and regulating fibroblast activation and myofibroblast differentiation via the TGF- $\beta$  pathway. C/EBP $\beta$ -deleted mice exhibited a decrease in  $\alpha$ SMA and ColI mRNA and protein levels and suppression of TGF- $\beta$ -induced fibroblast differentiation into myofibroblasts subsequent to attenuation of ECM accumulation and fibrosis<sup>17,18,35–37</sup>. In renal injury and disease, there is a consensus that the transformation of fibroblasts to myofibroblasts plays a pathological role in interstitial ECM accumulation during progressive tubulointerstitial fibrosis as assessed by upregulated expression of  $\alpha$ SMA and other related ECM proteins<sup>5,6,33,38</sup>. Although the origin of interstitial myofibroblasts during renal fibrosis is controversial, TGF- $\beta$ 1 is a key mediator activating various cells, such as tubular epithelial cells, resident fibroblasts, and bone marrow-derived mesenchymal stem cells whereby they lose their normal phenotypes and acquire a myofibroblast phenotype, accelerating matrix synthesis in renal fibrosis<sup>33,38,39</sup>. In our study, we found that TGF- $\beta$ 1 mRNA expression level was positively correlated with Saa3 promoter activity. This suggests that the increased bioluminescent signal intensity observed in Saa3 promoter-luc mice reflected differentiation and activation of myofibroblasts in tubulointerstitial fibrosis.

In this study, Saa3 gene promoter activity was applied to predict tubulointerstitial fibrosis in both chronic and acute renal injuries. Thus, the pathological relationship between Saa3 and kidney disease and fibrosis should be discussed. Recent studies coincidentally reported the upregulation of members of the Saa family in plasma and kidney tissues of patients and experimental animals having kidney disease<sup>20–25</sup>. Not solely in the kidney, Saa was also found to play a role in fibrosis in other organs, including the lung, pancreas, and liver, in which Saa3-deficient mice exhibited markedly reduced ECM and fibrosis and a positive correlation between Saa expression with fibrotic markers and fibrotic severity was observed<sup>20,40,41</sup>. Although molecular mechanisms of Saa in fibrosis development have been unclear, recent studies suggest its possible association with inflammatory-related pathways. Saa3 has been reported to be an endogenous ligand for toll-like receptor 4 (TLR4), a receptor recently found to be implicated in inflammation and fibrosis<sup>42,43</sup>. Thus, it is possible that Saa3 may exert its fibrotic function through activation of the TLR4 signaling pathway. In response to injury or inflammation, Saa is highly synthesized in local tissue<sup>21,44–46</sup>. In diabetic kidney disease (DKD), Saa was found to be expressed throughout the kidney and highly deposited in tubulointerstitial fibrotic areas in kidney tissues of both the patients and experimental animals<sup>21</sup>. Under diabetes-like conditions (exposure to advanced glycation products (AGE)), Saa and inflammatory mediators, such as C-X-C motif chemokine ligand 5 (Cxcl5), C-C motif chemokine ligand 2 (Ccl2), and C-C motif chemokine ligand 5 (Ccl5) were significantly upregulated in renal podocytes<sup>47</sup>. Notably, knocking out Saa3 significantly inhibited AGE-induced expressions of Cxcl5, Ccl2, and Ccl5 in podocytes, while exogenous addition of recombinant Saa protein upregulated Saa3 itself and inflammatory mediators associated with nuclear factor- $\kappa$ B (NF- $\kappa$ B) activation<sup>21,47</sup>. Taken together with the notion that Cxcl5, Ccl2, and Ccl5 are chemoattractants, these results indicate that Saa acted in a chemoattractive manner to modulate immune cell recruitment in injured or inflammatory sites in the kidney. Interestingly, some studies demonstrated that Saa was a connector binding ECM and immune cells, such as neutrophils, monocytes, T cells, and mast cells, providing cross talk between these cells and the accumulation of immune cells in inflammatory sites<sup>44,48</sup>. In the kidney, accumulation of immune cells and Saa in parallel with upregulation of TGF- $\beta$ 1 and  $\alpha$ SMA were found in interstitial fibrotic areas, leading to an assumption that the presence of immune cells and Saa enhanced renal fibrosis<sup>44</sup>. More recent works examined an important role of macrophage recruitment during the development of renal fibrosis<sup>49,50</sup>. It showed that the recruited macrophages were mainly M1 macrophages at early stage (three days after the UUO operation) and then were shortly polarized into M2 macrophages, which released high levels of TGF- $\beta$ 1 to promote renal fibrosis<sup>50</sup>. This work is consistent with previous studies suggesting that TGF- $\beta$ 1 was a key mediator, controlling the phenotypic transition of resident renal cells into myofibroblasts, leading to fibrosis<sup>33,38,39</sup>. Although these observations suggest the involvement of Saa3 in the renal fibrotic process via inflammatory-related pathways, further experiments are needed to clarify the causal relationship between bioluminescent signal visualized in Saa3 promoter-luc mice and immune cell recruitment.

Finally, we applied Saa3 promoter-luc mice for the *in vivo* non-invasive exploration of food factors preventing kidney disease in the adenine-induced kidney disease model. We found that G-Hes effectively prevented renal inflammation and fibrosis, which accompanied inhibition of DHA crystal deposition in renal tubules. We also found the inhibitory effect of its hydrolyzed form, hesperetin, on XOR activity *in vitro*. As XOR is a critical enzyme, catalyzing the oxidation of hypoxanthine to uric acid<sup>51</sup>, we can expect that G-Hes would be a food factor preventing hyperuricemia with excess uric acid in the blood. This study provides a novel approach to investigate effects of functional food by visualizing bioluminescent signal in Saa3 promoter-luc mice. As described above, Saa3 is highly expressed in tubulointerstitial fibrotic areas in kidney tissues of mouse DKD models, whereas previous reports have demonstrated that Saa3 facilitated pulmonary metastasis through stimulating NF- $\kappa$ B/TLR4 signaling pathways<sup>43,52</sup>. Taken together with these observations, Saa3 promoter-luc mouse model can be widely applied as an *in vivo* non-invasive model in exploring compounds or food factors for preventing not only DKD but also other diseases, such as cancer metastasis.

## Materials and Methods

**Establishment of Saa3 promoter-luc chimeric mice.** Saa3/C/EBP $\beta$ -promoter transgenic mouse carrying mouse Saa3 promoter region (–314/+50) upstream of the complete luciferase cDNA was generated as described previously<sup>12,13,16</sup>. In this experiment, heterozygous mice harboring the transgene which were backcrossed at least five times with purebred C57BL/6J mice (Charles River Japan, Kanagawa, Japan), and their control

littermates were used. Male CD-1 (ICR) mice (four weeks old) were from Charles River Japan. Mice were housed in groups of two or three in metal cages maintained at 24 °C with a 12-h light and dark cycle (lights on, 8:00 a.m. to 8:00 p.m.). MF solid chow (Oriental Yeast, Tokyo, Japan) and deionized water were provided *ad libitum*. The animal study was approved by the Hiroshima University Animal Committee (Permit Number: C13-3 and C18-2), and the mice were maintained in accordance with the Hiroshima University Guidelines for the Care and Use of Laboratory Animals.

**Adenine-induced and UO kidney injury experiments.** Male C57BL/6J mice (eight weeks old, Charles River Japan) as WT mice and Saa3 promoter-luc mice (5–8 weeks old, established in this study) were housed in groups of two or three in metal cages under the conditions described above. The control diet used in all experiments was composed of the following components (g/kg diet):  $\alpha$ -cornstarch, 402; casein, 200; sucrose, 200; corn oil, 100; cellulose, 50; AIN-93G mineral mixture, 35; AIN-93 vitamin mixture, 10; and L-cystine, 3, as described previously<sup>53</sup>.

For the adenine-induced kidney injury experiment, the adenine diet was composed of the control diet mixed with adenine (FUJIFILM Wako, Osaka, Japan) in a dose of 2 g adenine/kg diet (0.2% w/w). This adenine dose was chosen because it showed a survival rate of 100% with the renal injury phenotypes reported previously<sup>26</sup>. The G-Hes diet was composed of the control diet mixed with G-Hes (Hayashibara, Okayama, Japan) (3% w/w), while the G-Hes-mixed adenine diet was composed of the adenine diet mixed with G-Hes (3% w/w). Both WT mice and Saa3 promoter-luc mice were randomly divided into the control group receiving the control diet, the adenine group receiving the adenine diet, and the G-Hes group receiving G-Hes-mixed adenine diet for one, two, or three weeks. In the G-Hes group, mice were fed the G-Hes diet for 3 days before the start of the adenine treatment. For allopurinol experiment, the allopurinol group was given allopurinol (25 mg/kg/day; Sigma, St. Louis, MO) in the drinking water from 2 weeks after the start of the adenine treatment until end of the experiment (six weeks). At the end of each experiment, mice were sacrificed, and organs and blood were harvested. The *n* for each experimental group is defined within the figure legends.

For the UO kidney injury experiment, WT mice and Saa3 promoter-luc mice were randomly divided into the UO group or the sham group, and their left ureters were ligated with 6-G silk sutures, as previously described<sup>50,54</sup>. For sham operation, mice were treated the same way as UO mice, except the ligation. After surgery, mice were fed the control diet and then sacrificed at three or seven days as mentioned in the legends of figures.

**Plasmid construction, cell culture, and DNA transfection.** Mouse Saa3 promoter region (−314/+50) was ligated upstream of the luciferase cDNA in pGEM3 (Promega, Madison, WI, USA), generating pSaa3-Luc. pSaa3-Luc was digested with both *EcoRI* and *NotI*, and the resulting DNA fragment containing the mouse Saa3 promoter region (−314/+50) and luciferase cDNA (Saa3-Luc) was ligated into *EcoRI* and *NotI* sites of the pMX vector. Site-directed mutagenesis was performed using PrimeSTAR HS DNA Polymerase (TaKaRa Bio) as described previously<sup>12</sup>. The mutation was confirmed by DNA sequencing analysis. C/EBP $\beta$  cDNA was amplified using a PCR primer set (5′-CCGCGTTCATGCACCGCTG-3′ and 5′-ACCCGCGCCGCTAGCAGT-3′) and subcloned into pcDNA3.1, which generated pcDNA-C/EBP $\beta$ . The human proximal tubular cell line HK-2 was cultured in a maintenance medium (10% fetal bovine serum, 100 units/ml penicillin and 100  $\mu$ g/ml streptomycin in Dulbecco's modified medium with low glucose) at 37 °C in 5% CO<sub>2</sub>/95% humidified air. DNA transfections were performed using GeneJuice Transfection Reagent (Merck Millipore, Billerica, MA) according to the manufacturer's instructions. After DNA transfection into HK-2 cells, these cells were stimulated with 10 ng/ml of mouse recombinant tumor necrosis factor- $\alpha$  (R&D system, Minneapolis, MN) for 24 h.

**In vivo bioluminescence imaging analysis.** Male Saa3 promoter-luc mice were injected intraperitoneally with D-luciferin (150 mg/kg body weight, Promega) and then anesthetized with pentobarbital sodium (Kyoritsu Seiyaku, Tokyo, Japan). After five min, Saa3-luc mice were placed in a prone position on the plate and imaged for 1 min with the camera set at the highest sensitivity level by NightOWL II Imaging Systems LB983 (Berthold Technologies, Bad Wildbad, Germany), except the mice shown in Fig. 1e (they were placed in a supine position). Photons emitted from tissues were analyzed using Indigo *in vivo* image software (Berthold). Signal intensity was quantified as the sum of all detected photon counts per second and presented as count/sec (cps). For any given analysis, all images were adjusted to the same scale of minimum and maximum luminescent intensity.

**Ex vivo quantitative luciferase assay.** Tissues obtained from Saa3 promoter-luc mice were homogenized in the lysis buffer (1% Triton-X 100, 2 mM DTT, 10% glycerol, and 25 mM Tris-HCl pH 7.5), followed by centrifugation at 12,000 rpm, 4 °C, for 10 min and supernatant collection. For cell lysate, the cells were lysed in ice-cold lysis buffer. After sonication, cell lysate was centrifuged at 12,000 rpm and supernatant was collected. Luciferase activity was quantified using the luciferase assay kit (Toyo Inki, Japan) and a luminometer (Turner Model TD-20), expressed as relative light units normalized to total protein concentration of the cell or tissue extracts.

**RT-PCR analyses.** Total RNAs were isolated from kidney using RNeasy lipid tissue kit (Qiagen Sciences, Germantown, MD). The reverse transcriptase reaction was carried out with 1  $\mu$ g total RNA as a template to synthesize cDNA using ReverTra Ace (TOYOBO, Osaka, Japan) and random hexamers (TaKaRa Bio, Kyoto, Japan), according to the manufacturer's instructions. For semi-quantitative PCR analysis, cDNA and primers were added to the GoTaq Master Mix (Promega) to give a total reaction volume of 20  $\mu$ l. Reactions were sampled after 28 and 30 cycles under different PCR conditions, to monitor product accumulation. For quantitative PCR analysis, cDNA and primers were added to the THUNDERBIRD SYBR qPCR Mix (TOYOBO), to give a total reaction volume of 20  $\mu$ l. PCR reactions were then performed using StepOnePlus™ (Applied Biosystems, Foster City, CA). Conditions were set to the following parameters: 2 min at 95 °C, followed by 40 cycles each of 15 s at 95 °C and 1 min at 60 °C. The primers used for PCR analyses were as follows: Saa3, F, 5′-AAGGGTCTAGAGACATGTGG-3′, and R,

5'-ACTTCTGAACAGCCTCTCTG-3'; TNF- $\alpha$ , F, 5'-CCGAT GGGTTGTACCTTGTC-3', and R, 5'-CGGACTC CGCAAAGTCTAAG-3';  $\alpha$ SMA, F, 5'-GGCTCTGGGCTCTGTA-3', and R, 5'-CTCTTGCTCTGGGCT TCATC-3'; Col1, F, 5'-CCCAAGGAAAAGAAGC-3', and R, 5'-ACATTAGGCGCAGGAAGGTCA-3'; L19, F, 5'-GGC ATAGGGAAGAGGAAGG-3', and R, 5'-GGATGTGCTCCATGAGGATGC-3'; C/EBP $\beta$ , F, 5'-ACAAGCTGAG CGACGGTAC-3', and R, 5'-ACAGCTGCTCCACCT TCTTC-3'.

**Immunohistochemical analysis.** Kidney tissues were fixed in 4% paraformaldehyde. Paraffin sections of 4  $\mu$ m were stained with H&E and Azan-Mallory stain. For immunofluorescence staining in Fig. 2d,e (three or seven days of UOU) and Fig. 3c (two weeks of the adenine treatment) frozen kidneys were sliced with 5- $\mu$ m thickness. The slices were fixed with acetone or 4% paraformaldehyde. After blocking in 5% donkey serum for 30 min at room temperature, slices were incubated with primary antibody, followed by Alexa Fluor labeled (Molecular probe) secondary antibody. The images were captured by confocal microscopy (FV2000, Olympus) and were processed by Olympus fluoview ver.4.0. Antibodies of  $\alpha$ SMA (Cell Signaling, 1A4, 48939), E-Cad (Abcam, DECMA-1, ab11512), and CEBP $\beta$  (c-7962; Santa Cruz Biotechnology) were used.

**Western blot analysis.** Kidney tissues were homogenized in the lysis buffer (150 mM NaCl, 1% Nonidet P-40, 0.5% sodium deoxycholate, 0.1% SDS, 50 mM Tris-HCl, pH 7.4) followed by centrifugation at 12,000 rpm, 4 °C, for 10 min and supernatant collection. Protein concentration of the supernatant was determined using the Bio-Rad protein assay kit (Bio-Rad) with BSA as a standard. 20  $\mu$ g (protein equivalents) of the supernatant was resolved by SDS-PAGE, transferred onto a polyvinylidene difluoride (PVDF) membranes and immunoblotted with anti-CEBP $\beta$  (Santa Cruz Biotechnology) antibody.

**Plasma BUN and creatinine analysis.** BUN and creatinine were determined using a Beckman Coulter AU480 analyser (Beckman Coulter, Krefeld, Germany), which is an automated chemistry instrument for turbidimetric, spectro-photometric, and ion-selective electrode measurements. Briefly, 200  $\mu$ L plasma was used to measure these parameters according to the manufacturer's protocol.

**XOR activity analysis.** WT mice were randomly divided into the control group or the G-Hes group. Before starting the experiment, the G-Hes group was treated with G-Hes (500 mg/kg body weight) in saline solution by a single oral administration for 2 h, while the control group was treated with saline solution. After 2 h, all mice were treated with the uricase inhibitor, potassium oxonate (250 mg/kg *i.p.*, FUJIFILM Wako)<sup>55</sup> in saline solution. Blood samples (100  $\mu$ L each) were collected at 0, 0.5, 1, and 2 h after potassium oxonate injection by cutting the tail tip. Prior to G-Hes treatment, blood was also collected as the basal urate level. Plasma was obtained by centrifugation at 3000 rpm, for 10 min, and at 4 °C. Plasma urate levels were determined by high-performance liquid chromatography (HPLC) using a Cosmosil 5C<sub>18</sub>-PAQ (4.6  $\times$  250 mm; Nacalai Tesque, Kyoto, Japan) with an isocratic elution of 20 mM phosphate buffer (pH 2.5) at a flow rate of 0.5 ml/min, a temperature of 30 °C, and a monitored wavelength of 290 nm.

**Statistical analyses.** Values were presented as means  $\pm$  S.E. Statistical significance was determined by unpaired Student's *t* test. For all tests, the results with *p* < 0.05 were considered statistically significant.

## References

- Crews, D. C., Bello, A. K. & Saadi, G. Burden, access, and disparities in kidney disease. *Kidney Int.* **95**, 242–248 (2019).
- Fraser, S. D. S. & Roderick, P. J. Kidney disease in the Global Burden of Disease Study 2017. *Nat. Rev. Nephrol.* **15**, 193–194 (2019).
- Vanholder, R. *et al.* Reducing the costs of chronic kidney disease while delivering quality health care: A call to action. *Nat. Rev. Nephrol.* **13**, 393–409 (2017).
- Zhang, Q. L. & Rothenbacher, D. Prevalence of chronic kidney disease in population-based studies: Systematic review. *BMC Public Health* **8**, 117 (2008).
- Boor, P., Ostendorf, T. & Floege, J. Renal fibrosis: Novel insights into mechanisms and therapeutic targets. *Nat. Rev. Nephrol.* **6**, 643–656 (2010).
- Liu, Y. Cellular and molecular mechanisms of renal fibrosis. *Nat. Rev. Nephrol.* **7**, 684–696 (2011).
- Rohatgi, R. & Flores, D. Intratubular hydrodynamic forces influence tubulointerstitial fibrosis in the kidney. *Curr. Opin. Nephrol. Hypertens.* **19**, 65–71 (2010).
- Liu, B. C., Tang, T. T., Lv, L. L. & Lan, H. Y. Renal tubule injury: a driving force toward chronic kidney disease. *Kidney Int.* **93**, 568–579 (2018).
- Qi, R. & Yang, C. Renal tubular epithelial cells: the neglected mediator of tubulointerstitial fibrosis after injury. *Cell Death Dis.* **9** (2018).
- Gross, S. *et al.* Bioluminescence imaging of myeloperoxidase activity *in vivo*. *Nat. Med.* **15**, 455–461 (2009).
- Conway, J. R. W., Carragher, N. O. & Timpson, P. Developments in preclinical cancer imaging: Innovating the discovery of therapeutics. *Nat. Rev. Cancer* **14**, 314–328 (2014).
- Sanada, Y. *et al.* Serum Amyloid A3 Gene Expression in Adipocytes is an Indicator of the Interaction with Macrophages. *Sci. Rep.* **6**, 1–15 (2016).
- Geurts, J. *et al.* A novel Saa3-promoter reporter distinguishes inflammatory subtypes in experimental arthritis and human synovial fibroblasts. *Ann. Rheum. Dis.* **70**, 1311–1319 (2011).
- Ogasawara, K. *et al.* A serum amyloid A and LDL complex as a new prognostic marker in stable coronary artery disease. *Atherosclerosis* **174**, 349–356 (2004).
- Sattianayagam, P. T., Hawkins, P. N. & Gillmore, J. D. Systemic amyloidosis and the gastrointestinal tract. *Nat. Rev. Gastroenterol. Hepatol.* **6**, 608–617 (2009).
- Geurts, J. *et al.* Computational design and application of endogenous promoters for transcriptionally targeted gene therapy for rheumatoid arthritis. *Mol. Ther.* **17**, 1877–1887 (2009).
- Hu, B. *et al.* CCAAT/enhancer-binding protein isoforms and the regulation of alpha-smooth muscle actin gene expression by IL-1 beta. *J. Immunol.* **173**, 4661–4668 (2004).
- Hu, B., Wu, Z., Nakashima, T. & Phan, S. H. Mesenchymal-specific deletion of C/EBP $\beta$  suppresses pulmonary fibrosis. *Am. J. Pathol.* **180**, 2257–2267 (2012).

19. Rahman, S. M. *et al.* CCAAT/enhancer binding protein  $\beta$  deletion in mice attenuates inflammation, endoplasmic reticulum stress, and lipid accumulation in diet-induced nonalcoholic steatohepatitis. *Hepatology* **45**, 1108–1117 (2007).
20. Liu, T. *et al.* FIZZ2/RELM- Induction and Role in Pulmonary Fibrosis. *J. Immunol.* **187**, 450–461 (2011).
21. Anderberg, R. J. *et al.* Serum amyloid A and inflammation in diabetic kidney disease and podocytes. *Lab. Invest.* **95**, 250–262 (2015).
22. Hassoun, H. T. *et al.* Ischemic acute kidney injury induces a distant organ functional and genomic response distinguishable from bilateral nephrectomy. *Am. J. Physiol.* **293**, F30–F40 (2007).
23. Puthanveetil, P., Chen, S., Feng, B., Gautam, A. & Chakrabarti, S. Long non-coding RNA MALAT1 regulates hyperglycaemia induced inflammatory process in the endothelial cells. *J. Cell. Mol. Med.* **19**, 1418–1425 (2015).
24. Wu, D. *et al.* Downregulation of lncRNA MALAT1 contributes to renal functional improvement after duodenal-jejunal bypass in a diabetic rat model. *J. Physiol. Biochem.* **74**, 431–439 (2018).
25. Grigoryev, D. N. *et al.* The local and systemic inflammatory transcriptome after acute kidney injury. *J. Am. Soc. Nephrol.* **19**, 547–558 (2008).
26. Tanaka, T. *et al.* Urinary L-type fatty acid-binding protein can reflect renal tubulointerstitial injury. *Am. J. Pathol.* **174**, 1203–1211 (2009).
27. Zeisberg, M. & Neilson, E. G. Biomarkers for epithelial-mesenchymal transitions. *J. Clin. Invest.* **119**, 1429–1437 (2009).
28. Schmouder, R. L., Strieter, R. M., Wiggins, R. C., Chensue, S. W. & Kunkel, S. L. *In vitro* and *in vivo* interleukin-8 production in human renal cortical epithelia. *Kidney Int.* **41**, 191–198 (1992).
29. Sridharan, B., Mehra, Y., Ganesh, R. N. & Viswanathan, P. Regulation of urinary crystal inhibiting proteins and inflammatory genes by lemon peel extract and formulated citrus bioflavonoids on ethylene glycol induced urolithic rats. *Food Chem. Toxicol.* **94**, 75–84 (2016).
30. Minn, A. J. *et al.* Genes that mediate breast cancer metastasis to lung. *Nature* **436**, 518–524 (2005).
31. Kong, B. *et al.* Long non-coding RNA HOTAIR reprograms chromatin state to promote cancer metastasis. *Nature* **464**, 1071–1076 (2010).
32. Tominaga, N. *et al.* Brain metastatic cancer cells release microRNA-181c-containing extracellular vesicles capable of destructing blood-brain barrier. *Nat. Commun.* **6** (2015).
33. Hewitson, T. D. Renal tubulointerstitial fibrosis: common but never simple. *Am. J. Physiol.* **296**, F1239–F1244 (2009).
34. Houglum, K. *et al.* LAP (NF-IL6) transactivates the collagen alpha 1 (I) gene from a 5' regulatory region. *J. Clin. Invest.* **94**, 808–814 (1994).
35. Buck, M. & Chojkier, M. A ribosomal S-6 kinase-mediated signal to C/EBP- $\beta$  is critical for the development of liver fibrosis. *PLoS One* **2**, e1372 (2007).
36. Hu, B., Ullenbruch, M., Jin, H., Gharaee-Kermini, M. & Phan, S. An essential role for CCAAT/enhancer binding protein  $\beta$  in bleomycin-induced pulmonary fibrosis. *J. Pathol.* **211**, 455–462 (2007).
37. Buck, M. & Chojkier, M. C/EBP $\beta$  associates with caspase 8 complex proteins and modulates apoptosis in hepatic stellate cells. *J. Clin. Gastroenterol.* **41**, 295–299 (2007).
38. Böttinger, E. P. TGF- $\beta$  in renal injury and disease. *Semin. Nephrol.* **27**, 309–320 (2007).
39. Lebleu, V. S. *et al.* Origin and function of myofibroblasts in kidney fibrosis. *Nat. Med.* **19**, 1047–1053 (2013).
40. Djurec, M. *et al.* Saa3 is a key mediator of the protumorigenic properties of cancer-associated fibroblasts in pancreatic tumors. *Proc. Natl. Acad. Sci. USA* **115**, E1147–E1156 (2018).
41. Winkler, S. *et al.* Human mesenchymal stem cells towards non-alcoholic steatohepatitis in an immunodeficient mouse model. *Exp. Cell Res.* **326**, 230–239 (2014).
42. Bhattacharyya, S. *et al.* Toll-like receptor 4 signaling augments transforming growth factor- $\beta$  responses. *Am. J. Pathol.* **182**, 192–205 (2012).
43. Hiratsuka, S. *et al.* The S100A8-serum amyloid A3-TLR4 paracrine cascade establishes a pre-metastatic phase. *Nat. Cell Biol.* **10**, 1349–1355 (2008).
44. Toth, T., Toth-Jakatics, R., Jimi, S. & Takebayashi, S. Increased density of interstitial mast cells in amyloid a renal amyloidosis. *Mod. Pathol.* **13**, 1020–1028 (2000).
45. Meek, R. L. & Benditt, E. Amyloid a gene family expression in different mouse tissue. *J. Exp. Med.* **164**, 2006–2017 (1986).
46. Mitchell, T. I., Coon, C. I. & Brinckerhoff, C. E. Serum Amyloid A (SAA3) produced by rabbit synovial fibroblasts treated with phorbol esters or interleukin 1 induces synthesis of collagenase and is neutralized with specific antiserum. *J. Clin. Invest.* **87**, 1177–1185 (1991).
47. Dieter, B. P. *et al.* Serum amyloid A and Janus kinase 2 in a mouse model of diabetic kidney disease. *PLoS One* **14**, e0211555 (2019).
48. Preciado-Patt, L., Hershkoviz, R., Fridkin, M. & Lider, O. Serum amyloid A binds specific extracellular matrix glycoproteins and induces the adhesion of resting CD4+ T cells. *J. Immunol.* **156**, 1189–1195 (1996).
49. Tang, P. M. K., Nikolic-Paterson, D. J. & Lan, H. Y. Macrophages: versatile players in renal inflammation and fibrosis. *Nat. Rev. Nephrol.* **15**, 144–158 (2019).
50. Shen, B., Liu, X., Fan, Y. & Qiu, J. Macrophages regulate renal fibrosis through modulating TGF $\beta$  superfamily signaling. *Inflammation* **37**, 2076–2084 (2014).
51. Kamijo-Ikemori, A. *et al.* Renoprotective effect of the xanthine oxidoreductase inhibitor topiroxostat on adenine-induced renal injury. *Am. J. Physiol.* **310**, F1366–F1376 (2016).
52. Hiratsuka, S. *et al.* Primary tumours modulate innate immune signalling to create pre-metastatic vascular hyperpermeability foci. *Nat. Commun.* **4**, 1810–1853 (2013).
53. Kumrungsee, T. *et al.* Novel metabolic disturbances in marginal vitamin B6-deficient rat heart. *J. Nutr. Biochem.* **65**, 26–34 (2019).
54. Nakakuni, K., Matsuyama, M., Nomori, A., Fukushima, M. & Shimono, A. Secreted frizzled-related protein 1 (Sfrp1) regulates the progression of renal fibrosis in a mouse model of obstructive nephropathy. *J. Biol. Chem.* **289**, 31526–31533 (2014).
55. Fukunari, A. *et al.* Y-700 [1-[3-Cyano-4-(2,2-dimethylpropoxy)phenyl]-1H-pyrazole-4-carboxylic acid]: a potent xanthine oxidoreductase inhibitor with hepatic excretion. *J. Pharmacol. Exp. Ther. Copyr.* **311**, 519–528 (2004).

## Acknowledgements

This work was supported in part by grants from the Ministry of Education, Culture, Sports, Science, and Technology of Japan (to No. Y).

## Author Contributions

Th. K., Tai. K. and No. Y. designed the study. Th. K. and No. Y. wrote the paper. Tai. K., K. H., Y. S. and Na. Y. performed and analyzed most of the experiments. Tak. K. and M. M. designed and performed experiments shown in Figure 2. H. S. designed experiments shown in Figure 3. T. H. performed experiments shown in Figure 4c. F. A. J. V. designed the experiments shown in Figure 3e. All authors reviewed the results and approved the final version of the manuscript.



## Additional Information

**Supplementary information** accompanies this paper at <https://doi.org/10.1038/s41598-019-50685-0>.

**Competing Interests:** The authors declare no competing interests.

**Publisher's note** Springer Nature remains neutral with regard to jurisdictional claims in published maps and institutional affiliations.



**Open Access** This article is licensed under a Creative Commons Attribution 4.0 International License, which permits use, sharing, adaptation, distribution and reproduction in any medium or format, as long as you give appropriate credit to the original author(s) and the source, provide a link to the Creative Commons license, and indicate if changes were made. The images or other third party material in this article are included in the article's Creative Commons license, unless indicated otherwise in a credit line to the material. If material is not included in the article's Creative Commons license and your intended use is not permitted by statutory regulation or exceeds the permitted use, you will need to obtain permission directly from the copyright holder. To view a copy of this license, visit <http://creativecommons.org/licenses/by/4.0/>.

© The Author(s) 2019